NASA Technical Memorandum 106334

Damping Mechanisms in Chemically Vapor Deposited SiC Fibers

James A. DiCarlo and Jon C. Goldsby
Lewis Research Center
Cleveland, Ohio

Prepared for the
International Symposium on Damping of Multiphase Inorganic Materials
sponsored by the Physical Metallurgy and Composites Committee
Chicago, Illinois, November 2–5, 1992

NASA

DAMPING MECHANISMS IN CHEMICALLY VAPOR DEPOSITED SiC FIBERS

James A. DiCarlo and Jon C. Goldsby
National Aeronautics and Space Administration
Lewis Research Center
Cleveland, Ohio 44135

Abstract

Evaluating the damping of reinforcement fibers is important for understanding their microstructures and the vibrational response of their structural composites. In this study the damping capacities of two types of chemically vapor deposited silicon carbide fibers were measured from -200°C to as high as 800°C. Measurements were made at frequencies in the range 50 to 15000 Hz on single cantilevered fibers. At least four sources were identified which contribute to fiber damping, the most significant being thermoelastic damping and grain boundary sliding. The mechanisms controlling all sources and their potential influence on fiber and composite performance are discussed.

SILICON CARBIDE (SiC) FIBERS are among the leading candidates for reinforcement of metal and ceramic matrix composites. There is a strong need therefore to evaluate the properties of these fibers in order to anticipate composite performance. Of particular interest for vibrational and creep-sensitive composite applications are the damping of the fibers as a function of temperature and frequency. For example, the damping of a fiber-reinforced structural composite can be significantly enhanced by a fiber with high damping (1). In addition, composite creep can be controlled by the fiber creep which in the initial stages is related to fiber damping (2, 3).

The objectives of this investigation were two-fold. The first was to measure the damping capacity of two types of chemically vapor deposited (CVD) SiC fibers at temperatures and frequencies characteristic of composite applications. A single fiber vibration test was employed which allowed flexural damping measurements at temperatures from -200 to 800°C and at frequencies between 50 and 15000 Hz. This test also permitted measurement of the fibers' transverse thermal conductivity at room temperature. The second objective was to identify the underlying mechanisms that contribute to the fiber damping. Understanding damping mechanisms has both basic and technical implications because damping or internal friction is very sensitive to microstructural factors and thus can be utilized to detect possible internal changes within the fiber resulting from different fiber and composite fabrication and application conditions. For this reason, the fibers were tested in their as-received condition and after heat treatment at temperatures typical of metal and ceramic composite processing.

Experimental Procedure

The two types of SiC fiber monofilaments used in this study were obtained from Textron Specialty Materials, Lowell, MA. Trade names for these fiber types are SCS-6 and SCS-9 with nominal diameters of 143 μm and 75 μm, respectively. They were produced in multiple stages by chemical vapor deposition of SiC onto a 33 μm

Presented at the ASM Materials Congress/ TMS Fall Meeting; Symposium on Damping in Multiphase Inorganic Materials; November 4, 1992, Chicago, Ill.

carbon filament substrate. A detailed analysis of the complex microstructure of the SCS-6 fiber is given elsewhere (4). Generally the deposited SiC sheath of the as-received SCS-6 fiber consists of two primary zones: the inner zone being carbon-rich SiC and the outer zone being nearly stoichiometric SiC. The microstructure of the as-received SCS-9 sheath consists of one SiC zone which is chemically similar to that of the SCS-6 outer zone, that is, nearly stoichiometric (5). Both fiber types were produced with a carbon rich-coating of about 3 μm thickness (4). In order to simulate composite processing effects on fiber damping, some of the SCS-9 fibers were pre-annealed at 1000°C and 1400°C for 1 hour in an argon atmosphere.

A flexural test method was employed to measure fiber damping (6, 7). This approach was chosen because it provided maximum detection capability for a given fiber strain amplitude and also allowed the utilization of small fiber lengths, thereby allowing good control of fiber temperature and environment. For this test, a single cantilevered fiber was mounted in a metal clamp and electostatically driven at one of its lowest frequency flexural resonant modes. Fibers were cut with vibrational lengths from 10 to 50 mm which gave resonance frequencies within the audio range (2). When the excitation force was removed, the fiber's exponential free decay was monitored by an FM detection system and photographically recorded from an oscilloscope trace. The damping capacity ψ, which is the relative amount of mechanical energy lost per cycle, $\frac{\Delta W}{W}$, was calculated by

$$\psi = \frac{\Delta W}{W} = \frac{\ln a_1/a_2}{(f)(t_2 - t_1)} \qquad (1)$$

where decay amplitudes a_1 and a_2 were measured at times t_1 and t_2 and f is the resonance frequency. Strain amplitudes were kept below 10^{-5} to avoid strain-dependent damping. Measurements were also made in a vacuum of 10^{-6} Torr to eliminate the effects of air damping.

For a typical damping run, the fiber test system was placed in a cryostat, taken down to liquid nitrogen temperature (-195°C), and then allowed to slowly warm by electrical heating to 400°C. In some cases, the system was then placed into a separate furnace for elevated temperature runs to 800°C. The rate of temperature increase was about 3°C per minute. For each warm-up run, the fiber resonant frequency decreased slightly with increasing temperature. Decay traces were typically recorded every 5 to 10°C.

In a previous study (7) using the same methodology employed here, it was demonstrated that the total flexural fiber damping ψ can arise from a variety of sources; that is,

$$\psi = \psi_M + \psi_{TE} + \psi_o. \qquad (2)$$

Here ψ_M is due to intrinsic mechanisms within the fiber microstructure, ψ_{TE} is due to the classic thermoelastic effect for flexural vibrations (8), and ψ_o is due to experimental artifacts typically related to energy losses within the fiber clamp. Since one of the prime objectives of this study was to determine the mechanisms responsible for ψ_M, it was important to understand the ψ_{TE} and ψ_o contributions as a function of key experimental variables, such as test temperature, vibration frequency, and fiber diameter.

Generally ψ_o is quite small and typically assumed negligible. For this study, an upper limit for ψ_o of 2×10^{-4} was estimated under conditions where ψ_{TE} and ψ_M appeared to be zero (see later discussion). This limiting value was assumed to be independent of test and material conditions.

The thermoelastic damping ψ_{TE} on the other hand is strongly dependent on temperature, frequency, and fiber diameter (8). It arises because during flexure, thermal gradients are generated transversely across the fiber cross-section. If the vibrational period of the stress is near the relaxation time for thermal diffusion across the specimen thickness, mechanical energy losses arise. For a fiber specimen of cylindrical cross section, thermoelastic damping capacity is given by

$$\psi_{TE} = \psi_{TE\,max}[2ff_o/(f^2 + f_o^2)] \qquad (3)$$

where

$$\psi_{TE\,max} = \frac{\pi E \alpha^2 T}{\rho C} \qquad (4)$$

and

$$f_o = \frac{2.16k}{\rho C d^2}. \qquad (5)$$

Here C, ρ, d, E, α, k, T are the specific heat, density, diameter, axial Young's modulus, axial thermal expansion coefficient, effective transverse thermal conductivity, and average absolute temperature of the fiber, respectively. From Eq. 3, if f is more than an order of magnitude different than f_o , ψ_{TE} will make a negligible contribution to the total measured flexural damping. However if $f \cong f_o$, ψ_{TE} may contribute significantly and must be taken into account. In some cases, the appearance of ψ_{TE} can be useful because by Eqs. 3 and 5, measurement of the frequency $f = f_o$ which produces the greatest ψ_{TE} should then allow a determination of the fiber effective transverse thermal conductivity (7).

Results

SCS-6 Total Damping. Figure 1 shows the flexural damping versus temperature results for an as-received SCS-6 fiber at three resonant frequencies. Best fit curves are displayed because actual data points were almost continuous in nature and displayed a scatter of less than ± 5%. As can be seen , there was a strong frequency dependence for ψ at high temperature plus evidence of a small peak below 20°C. For all test conditions, total damping capacity of the SCS-6 fiber was less than 1%.

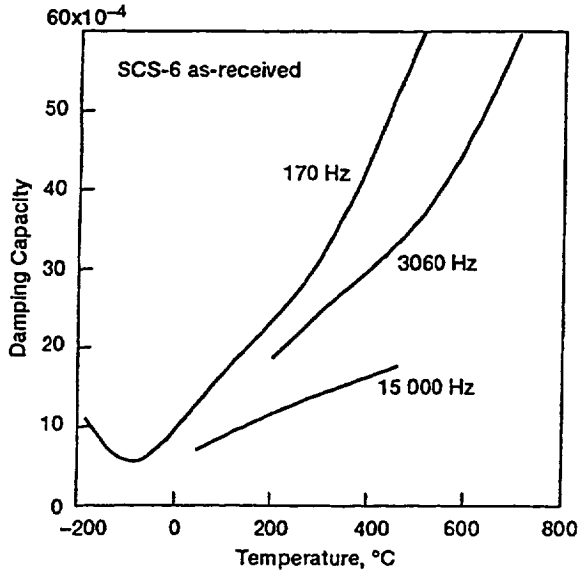

Figure 1.—Total flexural damping for as-received SCS-6 fibers.

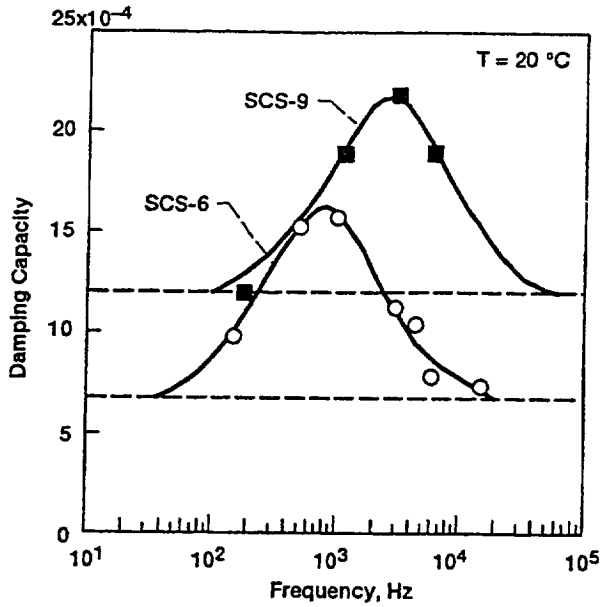

Figure 2.—Total flexural damping at 20 °C versus frequency for as-received fiber.

To understand and eliminate the thermoelastic contribution ψ_{TE} from the data of Fig. 1, damping was measured as a function of frequency at room temperature for both as-received SCS-6 and SCS-9 fibers. The results given in Fig. 2 show that each fiber type displayed a broad peak in the damping versus frequency plots, but that the peak maximum was at a higher frequency for the SCS-9 fiber. Assuming that the peaks were caused by the thermoelastic effect and that ψ_M was effectively frequency independent at room temperature, Eqs. 3 and 4 were fitted to each data set to yield the solid curves shown in Fig. 2 (c.f. Appendix). The good fit of these curves to the data not only confirms the contribution of the thermoelastic effect but also provides other insights.

For example, because of the low microstructural damping of the SCS type fibers, the thermoelastic effect in certain frequency ranges can make a major contribution to fiber damping when measured in flexure. By Fig. 2 and Eq. 4, $\psi_{TE_{max}}$ at room temperature was about 9×10^{-4}. This value is of the same order of magnitude as the estimated room temperature ψ_M values indicated by the horizontal lines on the low and high frequency sides of the thermoelastic peaks. On the other hand, Fig. 2 suggests that near room temperature, flexural data taken at frequencies below 100 Hz or above 10^5 Hz would have small ψ_{TE} contributions and thus would be directly indicative of ψ_M for both the SCS -6 and SCS-9 fibers.

Another observation from Fig. 2 is the magnitude of the center frequencies f_o for the SCS-6 and SCS-9 thermoelastic peaks. The fact that f_o differed by about a factor of four should be expected from Eq. 5 if both fiber types had the same effective transverse conductivity but differed only because of their diameters (a factor of about two). Using Eq. 5 and literature values for the various materials parameters (c.f. Appendix), it was determined that k for both the SCS-6 and SCS-9 fibers was about 0.04 cal/cm sec °C at 20°C.

SCS-6 Microstructural Damping. To determine the microstructural damping ψ_M for the SCS-6 fiber, the Fig. 1 results were corrected by removing the best estimates for the ψ_{TE} and ψ_o contributions. For ψ_{TE}, the Fig. 2 results were used for the room temperature correction; whereas the theoretical Eqs. 3, 4, and 5 and appropriate values for the material parameters were used for the corrections at other temperatures (c.f. Appendix). The temperature- dependent ψ_M results at 3060 Hz are shown by the dashed curve in Fig. 3 for the as-received SCS-6 fiber.

In analyzing the Fig. 3 results, it was observed that ψ_M between ~ 20 and 500 °C was effectively frequency independent, but monotonically increased with temperature. As will be discussed, this behavior is characteristic of the high temperature background damping seen in many materials (2). Below 20°C and above 500°C, however, ψ_M showed frequency dependencies characteristic of damping relaxation peaks (2). Below 20°C, for example , the as-received SCS-6 fiber appeared to display a small peak with ~ 14 x10^{-4} height near -200°C. Above 500°C, the fiber displayed the low temperature side of an apparently large relaxation peak. As will be discussed, this high temperature peak is characteristic of the grain boundary relaxation peak seen in polycrystalline materials.

Based on the above observations, it would appear that at least three mechanisms contribute to the general microstructural damping ψ_M of SCS- type fibers; that is,

$$\psi_M = \psi_{LTP} + \psi_{GB} + \psi_B \,. \qquad (6)$$

Here ψ_{LTP} is the damping from the source contributing to the low temperature peak, ψ_{GB} is the grain boundary damping peak, and ψ_B is due to the frequency-independent background damping which operates at all temperatures. Empirically it has been observed by

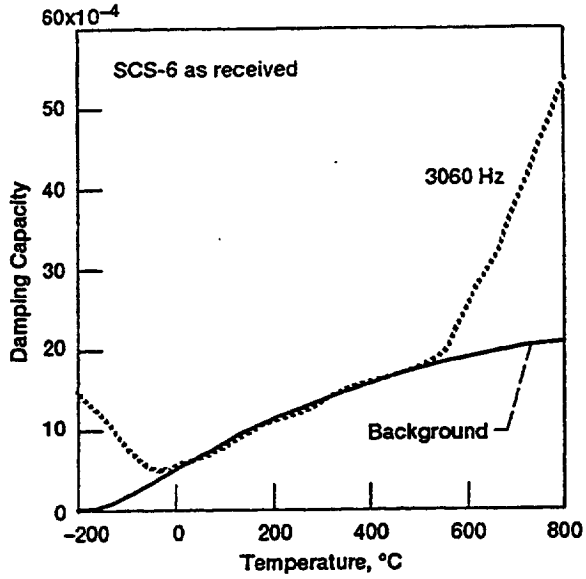

Figure 3.—Microstructural damping for as-received SCS-6 fibers. Solid curve is the estimated frequency-independent background damping.

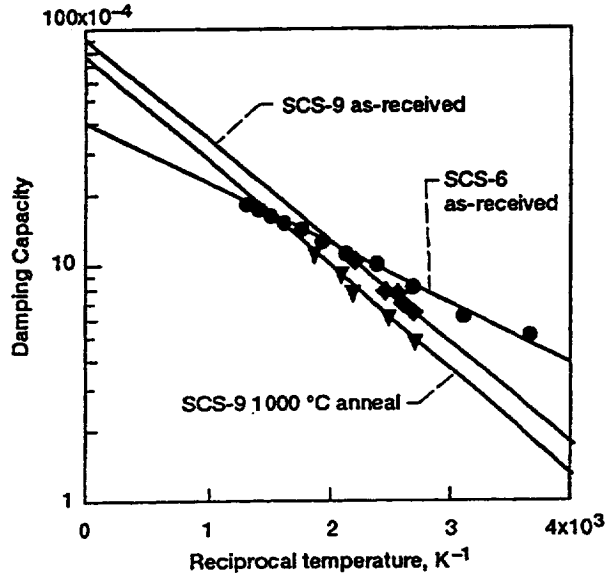

Figure 4.—Microstructural background damping for as-received and annealed SCS fibers.

TABLE I. Empirical Constants for Background Damping

	SCS-6 AS-RECEIVED	SCS-9 AS-RECEIVED	SCS-9 1000 °C ANNEAL
A x 10^4	36.7	89.6	75
C, kJ/mol	4.7	8.3	8.5

others (2) that the temperature dependence of ψ_B can be described by

$$\psi_B = Ae^{(-C/RT)}. \quad (7)$$

Here A and C are empirical constants and R= 8.314 J/mol·K is the universal gas constant. Assuming Eq. 7 also applies to the fibers of this study, the logarithm of the SCS-6 ψ_M results from 20 to 500°C were plotted versus 1/T in Fig. 4. The good fit of the data points to a straight line suggests that Eq. 7 can indeed be used to describe ψ_B for the as-received SCS-6 fibers. Using the best fit values for A and C constants given in Table I, it was then possible to draw the solid ψ_B curve labeled background in Fig. 3. In so doing, one can better appreciate the quantitative height of low and high temperature relaxation peaks.

SCS-9 Damping. Figure 5 shows the total flexural damping versus temperature results for an as-received SCS-9 fiber at two resonant frequencies. For this fiber type, data was taken only up to ~ 400°C in order to study the behavior of the low temperature relaxation peak and the background damping. Comparing Fig. 5 with the Fig. 1 results from the SCS-6 fiber, one can see that there is evidence for the low temperature peak in the SCS-9 fiber, but the behavior above 20°C is again complicated by the thermoelastic effect contribution. The opposite dependence of damping with increasing frequency for the two fibers types can be explained by the Fig. 2 results which show that because of the fiber diameter, the SCS-9 fiber data were taken on the low frequency side of the thermoelastic peak, whereas the SCS-6 data were taken primarily on the high frequency side.

Assuming Eq. 2 and correcting for the ψ_o and ψ_{TE} contributions (c.f. Appendix), the calculated temperature-dependent ψ_M results for the as-received SCS-9 fiber are plotted as the dashed curve in Fig. 6 at a frequency of 200 Hz. As with the SCS-6 fiber, the low temperature damping was found to be frequency dependent , whereas the monotonically increasing damping above 100°C was essentially frequency independent. Assuming this latter behavior could be described by Eq. 7, the Fig. 6 data

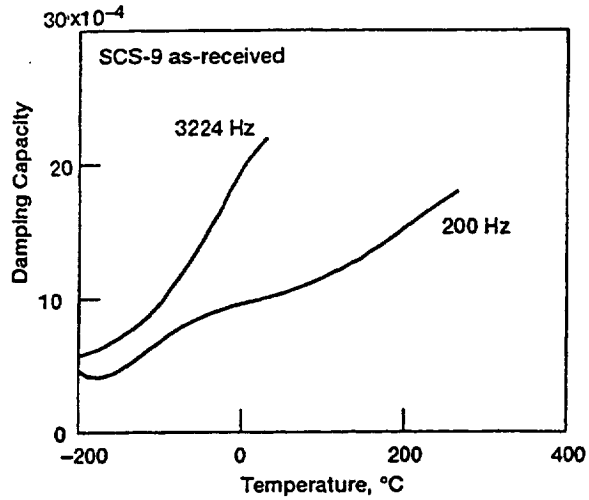

Figure 5.—Total flexural damping for as-received SCS-9 fibers.

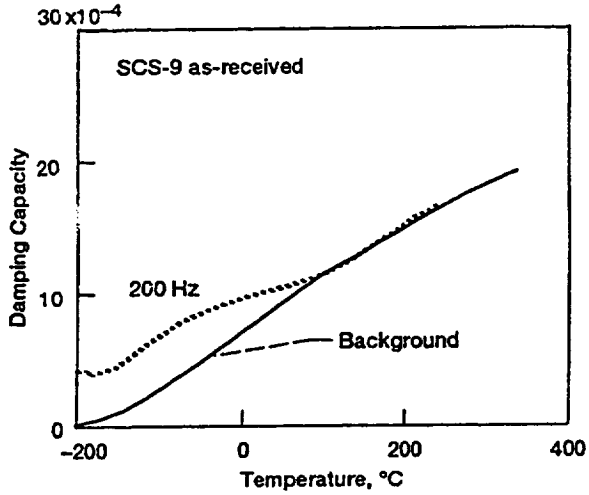

Figure 6 Microstructural damping for as-received SCS-9 fibers. Solid curve is estimated frequency-independent background damping.

between 100 and 300 °C were re-plotted in Fig. 4 to determine the empirical constants A and C. Using the values in Table I, the solid background curve shown in Fig. 6 was calculated. With this curve, one can better observe that the low temperature peak for the SCS-9 fiber was lower in height and extended over a broader temperature range than that for the SCS-6 fiber shown in Fig. 3.

Annealing Effects. To understand the effects of composite processing conditions on the damping capacities of the SCS type fibers, flexural damping was measured from -200 to 400°C for the SCS-9 fibers after they were annealed for one hour at 1000°C and 1400°C. The results shown in Fig. 7 were taken at ~200 Hz. Since this frequency is effectively out of the range where major ψ_{TE} contributions can occur , the Fig. 7 data was assumed to be equivalent to ψ_M data for the SCS-9 fibers.

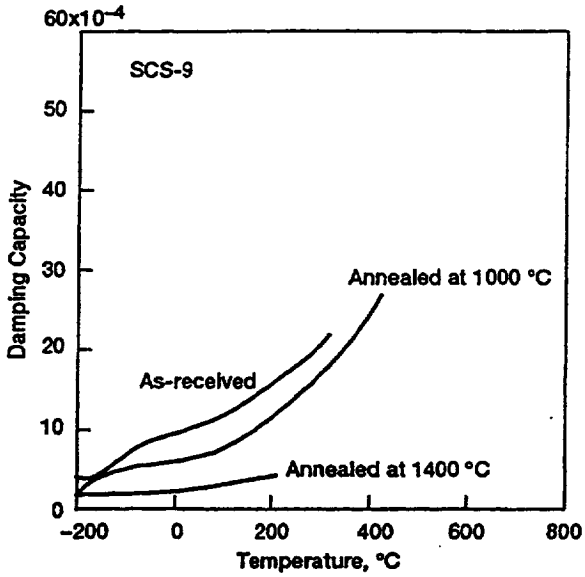

Figure 7.—Annealing effects on microstructrual damping for SCS-9 fibers.

Examining Fig. 7, one can see that the general effect of annealing was to significantly reduce the total microstructural damping at low temperatures. The major effect was in the reduction of the background ψ_B which after the 1400°C anneal was effectively zero. The remaining damping of $\sim 2 \times 10^{-4}$ is interpreted only as artifact damping ψ_o. As ψ_B decreased with annealing, it would appear from Fig. 4 and Table I that the controlling energy constant C remained unchanged but the empirical constant A decreased. A second annealing effect was the reduction of the low temperature damping. Although the data are insufficient to describe this reduction in any detail, they did show effectively no ψ_{LTP} after the 1400°C anneal. Thus after this exposure, the total microstructural damping for the SCS-9 fiber between -200 and 200°C was essentially zero (less than 1×10^{-4}).

Discussion

The flexural damping capacity results of this study show that for the temperature range -200 to 800 °C, the SCS-6 and SCS-9 fiber display at least four sources of damping. Three of these are associated with mechanisms within the fiber microstructures and thus are independent of the manner in which the vibrational stress is applied. These include the mechanisms responsible for (i) the small damping peak below 20°C, (ii) the background damping which predominates from ~20 to 500°C, and (iii) the large grain boundary damping peak whose low temperature side begins above 500°C. Because of the flexural test method, the strongly temperature and frequency dependent damping contribution associated with the thermoelastic effect was also observed. In the following discussion, these effects are examined in terms of their possible underlying mechanisms and practical implications for fiber and composite performance.

For the fiber microstructural damping, it is difficult to find evidence which directly identifies the actual mechanism responsible for each damping effect. The approach taken here will therefore be to suggest mechanisms based on the known microstructure and to discuss whether the proposed mechanisms are supported by the experimental facts. Since damping effects are generally related to microstructural defects, such as impurities, dislocations, and grain boundaries, one can examine the CVD SiC fiber microstructure for these defects and determine whether their presence can be correlated with a particular damping phenomenon. For example, it is known that SCS-6 and SCS-9 fibers are not only polycrystalline with grain sizes from 50 to 150 nm but are also chemically inhomogeneous. The SCS-6 fiber contains free carbon within the grain boundaries in the inner regions near the carbon substrate (4). In addition, there is evidence that free silicon can exist in the outer regions of the fibers. This evidence is based on (i) a fiber thermal expansion anomaly near the melting point of free silicon (9), (ii) an energy value controlling fiber creep which is near that associated with lattice diffusion in bulk silicon (9), (iii) creep reduction when the fiber is annealed above 1000°C, a temperature region in which rapid diffusion occurs in bulk silicon (9), (iv) chemical vapor deposition studies which suggest that at the lower temperatures at which the outer fiber regions are produced (~1000°C), free silicon is likely to be deposited (10), and

(v) rapid grain growth above 1400°C in the outer fiber region which is significantly greater than that of the inner fiber regions (5).

In light of the above discussion and because the flexural test method is more sensitive to microstructural effects in the outer fiber regions, it is suggested here that free silicon and grain boundaries were the primary defects responsible for microstructural damping effects in the SCS fibers. Thus the low temperature peak structures might be associated with point defect relaxations involving silicon impurity atoms. During fiber deposition, these atoms may have been frozen-in some disordered region within the fiber grain boundaries. During the flexural vibration, interaction between the mechanical stress and the thermal vibrations of these silicon atoms gave rise to damping peaks whose heights were proportional to the silicon content. Annealing the fibers at temperatures above 1000°C allowed solid state diffusion of these atoms to occur which in turn permitted their elimination and the disappearance of the low temperature peaks. Additional inferences from this model are that based on peak height (c.f. Figs. 3 and 6) , the free silicon content in the SCS-6 fiber may be greater than that of SCS-9 fiber and that fibers produced with greater silicon content (e.g., at lower deposition temperatures) may display larger low temperature damping peaks.

For the background damping, the apparent frequency independence of ψ_B does not allow simple interpretation in terms of typical relaxation phenomena. Since background damping has been observed in many materials, including single crystals, and is still not clearly understood (2), its source in the SCS fibers cannot as yet be clearly identified. The fact, however, that ψ_B disappeared with annealing above 1000°C suggests that it also may be associated with free silicon. That is, free silicon may be required either for its operation or for its removal. Clearly more studies are required which attempt to correlate microstructural variances with the background damping effects observed in Fig. 4 and Table I.

The mechanism responsible for the large rise in damping above 500°C (cf. Fig. 3) is assumed to be that of grain boundary relaxation. As is the general case for polycrystalline materials, a large damping peak is observed whenever the period of the mechanical vibration is near the relaxation time for grains to slide small distances relative to each other (2). In his classic studies on polycrystalline aluminum, Ke (3) observed that besides displaying a large damping peak, the grain boundary sliding mechanism also gave rise to measurable macroscopic creep and stress relaxation in aluminum. Thus the observance of the grain boundary peak above 500°C in the SCS-6 fiber implies evidence of the onset of creep. The fact that creep can occur at such a low temperature in this fiber was recently demonstrated through stress relaxation studies which showed measurable time-dependent deformation in SCS-6 fiber at or below 900°C (11). The controlling energy was observed to be near that of self-diffusion in bulk silicon.

To put the above results and discussion into practical perspective for vibrating composites, the fiber contribution to composite damping will depend not only on the fiber's damping mechanisms but also on the fiber's stored energy relative to that of the matrix (1). For example, for a unidirectional composite vibrated in tension, the axial composite damping capacity ψ_{11} can be estimated from

$$\psi_{11} = \gamma_{11}\psi_f + (1-\gamma_{11})\psi_m \qquad (8)$$

where ψ_f and ψ_m are the fiber and matrix damping capacities, respectively, and

$$\gamma_{11} = V_f \frac{E_f}{E_{11}}. \qquad (9)$$

Here V_f and E_f are the fiber volume fraction and modulus, respectively, and E_{11} is the composite axial modulus. Assuming for the purposes of discussion 40 volume percent of SCS-6 fiber in a titanium matrix, then $\gamma_{11} \cong 0.70$ so that the fiber damping in Eq. 8 is weighted significantly more than that of the matrix. However, because of their low microstructural damping, especially after exposure to thermal conditions simulating composite processing, the SCS fibers can only degrade rather than enhance composite damping. For example, assuming $\psi_f = 0$, then from Eq. 8 the SiC/Ti composite will effectively display a damping capacity only about 30% that of the matrix alone.

If a need arises to improve the microstructural damping of the CVD fibers and their composites, one possible approach based on the mechanisms suggested here would be to increase the silicon content of the fibers. However, the possible deleterious effects of the free silicon such as increased fiber creep and reaction with the matrix plus the probability of silicon removal during composite fabrication would appear to obviate this approach.

Another possibility is that within the fibers' inner regions, there can exist additional damping mechanisms which were not detected with the flexural test method used in this investigation. This is unlikely, however, because there is evidence that due to the carbon within the grain boundaries, the inner regions are significantly more creep and grain growth resistant than the outer regions (11,5). In addition, SiC/Ti composite damping results (12) in which the fibers were axially vibrated showed very low damping consistent with Eq. 8 and the results of Figs. 3 and 6.

One final point concerns the potential of utilizing the thermoelastic damping of the SCS fibers in order to enhance composite damping. If possible, this mechanism would not only contribute damping greater than the microstructural sources (cf. Fig. 2 and Appendix) but also would not change with composite use conditions. Although this mechanism should not be expected to operate for axial composite vibrations, one might speculate that for transverse vibrations and dissimilar conductivities between the fiber and matrix, thermal gradients could be generated across the fiber diameter. The interaction of these gradients with thermal waves traveling transversely in the fiber might then result in thermoelastic damping effects within the composite microstructure. However, as discussed in the Appendix, the maximum thermoelastic damping capacity to be expected from SiC fibers is still less than 1%.

Conclusions

The application of a flexural vibration test to chemically vapor deposited SCS-6 and SCS-9 fibers has allowed measurement of fiber damping capacities from -200 to 800°C and from 50 to 15000 Hz. Within these test conditions, at least four different damping mechanisms were detected and analyzed. Of those related to fiber microstructure, grain boundary relaxation was clearly the largest contributor. However, this mechanism began to operate only at temperatures above 500°C so that from a practical point of view, the general behavior of each fiber type was that of an elastic material with effectively zero damping. Free silicon is suggested to play a role in the other microstructural damping mechanisms, but apparently is eliminated under conditions simulating metal and ceramic composite processing. Finally, because of the flexural vibrational conditions, a damping contribution due to the thermoelastic effect was also detected. At certain frequencies and temperatures, the SCS fiber diameters were such as to allow the damping contribution due to this effect to be equivalent to or greater than those due to the microstructural mechanisms. Although the thermoelastic damping available in SiC fibers is not large enough to sufficiently enhance composite damping, it can be exploited, as was done in this study, to measure important fiber physical properties such as fiber transverse thermal conductivity. Thus the flexural damping measurement approach employed here can be useful not only to evaluate fiber damping mechanisms and their microstructural sources such as grain boundaries and impurities, but also to determine other fiber properties of technical interest.

References

1. DiCarlo, J. A. and Maisel J. E., Composite Materials: Testing and Design 5th Conf. STP 674, ed. S. W. Tsai, (ASTM, Philadelphia, Pa. 1979) 201-227
2. Nowick A. S. and Berry B. S., Anelastic Relaxation in Crystalline Solids, (Academic Press, New York and London 1972)
3. Ke, T.S., Phys. Rev. 71, (1947), 533-546
4. Ning, X. J. and P. Pirouz, J. Mat. Res. 6(10), (1991), 2234-2246
5. Bhatt, R. T. and Hull D. R., NASA Tech. Memo. 103772
6. Lesieutre, G.A., Eckel A. J., and DiCarlo J.A., Carbon 29(7) (1991), 1025-1032
7. DiCarlo, J. A. and Williams W., Ceramic Eng. & Sci. Proceedings, 1 (7-9), (1980), 671-691
8. C. Zener, Elasticity and Anelasticity of Metals, (The University of Chicago Press, Chicago 1948)
9. DiCarlo, J. A., J. Mat. Sci. 21, (1986), 217-224
10. Von Muench, W. and Pettenpaul E., J. Electrochem. Soc. 125 (2), (1978), 294-299
11. Morscher, G. N., DiCarlo J.A., and Wagner T. C., Ceramic. Eng.Sci. Proc., 12(7-8) (1991), 1032-1038
12. DiCarlo, J.A., and Maisel J.E., Adv. Fiber and Composites for Elevated Temperatures, eds. I. Ahmad and B.R. Norton, (The Metallurgical Society, Warrendale, Pa. 1980), 55-79
13. DiCarlo, J.A., Whisker and Fiber-Toughened Ceramics, (ASM International, Metals Park,OH 1988), 1-8
14. Thermophysical Properties of High Temperature Solid Materials, Vol. 5, ed. Y.S. Toulakian, (McMillian Co., New York. 1967)

Appendix: Thermoelastic Damping

To calculate the thermoelastic damping contribution to the flexural damping of the SCS- type fibers, Eq. 3, 4, and 5 were employed using literature values for the appropriate fiber parameters. For example, for the maximum thermoelastic damping $\psi_{TE_{MAX}}$ of the SCS-6 fiber, measured values for the fiber elastic modulus and axial thermal expansion were obtained from Ref. 13, whereas the fiber density and specific heat were calculated from the rule of mixtures using known dimensions for the SiC sheath and the carbon core (4) and temperature-dependent SiC and carbon specific heat data from Ref. 14. The net temperature dependence for the maximum thermoelastic damping as calculated by Eq. 4 is plotted in Fig. A-1 for the as-received SCS-6 fibers.

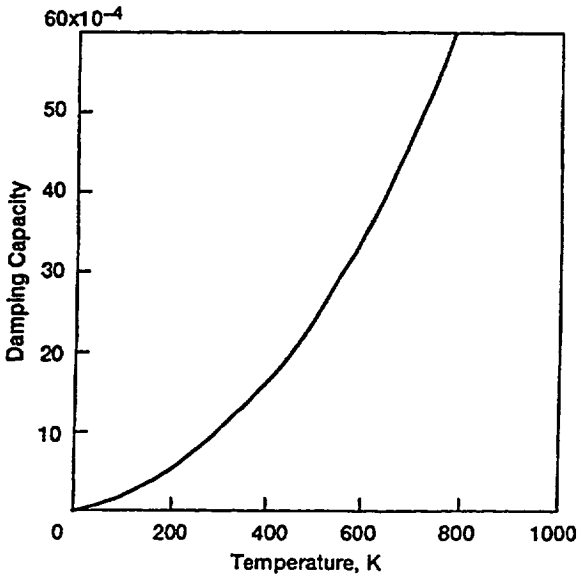

Figure A-1.—Maximum predicted thermoelastic damping for SCS-6 fibers.

Confirmation that the Fig. A-1 plot is accurate can be found in the frequency- dependent flexural damping of the as-received SCS-6 fiber as measured at room temperature. As shown in Fig. 2 the theoretical thermoelastic peak described by Eq. 3 was fitted to these data (open circles) using the calculated 20°C value for $\psi_{TE_{MAX}}$ of 9×10^{-4}. The excellent agreement of the peak to the data in both shape and height not only verifies use of Eq. 3 and the Fig. A-1 curve but also allows calculation and elimination of the thermoelastic contribution from the SCS fiber flexural damping at all frequencies and temperatures.

One complicating factor in the above analysis could be a shift of the center frequency f_0 which as described by Eq. 5 may change due to a net temperature dependence in the fiber's specific heat and /or transverse thermal conductivity. However, from -100 to 800°C, it has been observed that the transverse thermal conductivities of CVD SiC fibers and bulk materials remain fairly constant (7). Thus the only major temperature- dependent term in Eq. 5 is the fiber's specific heat which approximately doubles in this temperature range (14). Therefore, in using Eq. 3, the center frequencies (f_0) from -100 to 800°C were assumed to decrease inversely with specific heat, ranging from 1500 to 600 Hz for the SCS-6 fiber and from 6000 to 2400 Hz for the SCS-9 fiber.

REPORT DOCUMENTATION PAGE

Form Approved
OMB No. 0704-0188

1. AGENCY USE ONLY (*Leave blank*)	2. REPORT DATE	3. REPORT TYPE AND DATES COVERED
	July 1993	Technical Memorandum

4. TITLE AND SUBTITLE

Damping Mechanisms in Chemically Vapor Deposited SiC Fibers

5. FUNDING NUMBERS

WU–510–01–50

6. AUTHOR(S)

James A. DiCarlo and Jon C. Goldsby

7. PERFORMING ORGANIZATION NAME(S) AND ADDRESS(ES)

National Aeronautics and Space Administration
Lewis Research Center
Cleveland, Ohio 44135–3191

8. PERFORMING ORGANIZATION REPORT NUMBER

E–7697

9. SPONSORING/MONITORING AGENCY NAME(S) AND ADDRESS(ES)

National Aeronautics and Space Administration
Washington, D.C. 20546–0001

10. SPONSORING/MONITORING AGENCY REPORT NUMBER

NASA TM-106334

11. SUPPLEMENTARY NOTES

Prepared for the International Symposium on Damping of Multiphase Inorganic Materials sponsored by the Physical Metallurgy and Composites Committee, Chicago, Illinois, November 2–5, 1992. Responsible person, James A. DiCarlo, (216) 433–5514.

12a. DISTRIBUTION/AVAILABILITY STATEMENT

Unclassified - Unlimited
Subject Category 24

12b. DISTRIBUTION CODE

13. ABSTRACT ***(Maximum 200 words)***

Evaluating the damping of reinforcement fibers is important for understanding their microstructures and the vibrational response of their structural composites. In this study the damping capacities of two types of chemically vapor desposited silicon carbide fibers were measured from −200°C to as high as 800°C. Measurements were made at frequencies in the range 50 to 15000 Hz on single cantilevered fibers. At least four sources were identified which contribute to fiber damping, the most significant being thermoelastic damping and grain boundary sliding. The mechanisms controlling all sources and their potential influence on fiber and composite performance are discussed.

14. SUBJECT TERMS

Silicon carbide; Fibers; Damping capacity; Internal friction

15. NUMBER OF PAGES

11

16. PRICE CODE

A03

17. SECURITY CLASSIFICATION OF REPORT	18. SECURITY CLASSIFICATION OF THIS PAGE	19. SECURITY CLASSIFICATION OF ABSTRACT	20. LIMITATION OF ABSTRACT
Unclassified	Unclassified	Unclassified	